Available online at www.sciencedirect.com
ScienceDirect
Colloids and Surfaces A: Physicochem. Eng. Aspects 294 (2007) 117–129
COLLOIDS AND SURFACES A
www.elsevier.com/locate/colsurfa

Small-angle neutron scattering of silica nanoparticles templated in PEO–PPO–PEO cubic crystals

Danilo C. Pozzo, Lynn M. Walker*

Department of Chemical Engineering, Center for Complex Fluids Engineering, Carnegie Mellon University, Pittsburgh, PA 15213, USA

Received 14 October 2005; received in revised form 27 July 2006; accepted 2 August 2006
Available online 9 August 2006

Abstract

Small-angle neutron scattering (SANS) is used to characterize self-assembled nanocomposites. Thermo-reversible block-copolymer cubic crystals (Pluronic® F127) are used as three-dimensional templates to control the spatial arrangement of silica nanoparticles. The particles are dispersed in the block-copolymer phase and are organized by excluded volume interactions as they are driven into the interstitial cavities of the micelle cubic crystal. The technique of contrast variation is used to evaluate the structure of the templated nanoparticle array and the micelle crystal as a function of relative size, relative concentration and temperature. We show that shearing the samples results in macroscopic alignment of both the micelle cubic crystal and the templated particles. We use this highly ordered state to verify the feasibility of this templating approach. Through a study of control parameters, we find that templating is most effective at silica concentrations below the stoichiometric ratio of one particle per available template site. Higher polymer concentrations in the matrix and temperature above, but near, the order–disorder transition are also found to be favorable conditions for nanoparticle templating. The level of order of the cubic template is also found to be affected by the addition of the particles. At low silica concentrations, particle addition increases the long-range cubic order while at higher concentrations particle addition promotes disorganization. At a high polymer concentrations (30 w%), the addition of silica nanoparticles is also shown to trigger a change from a face-centered cubic (FCC) to a body-centered cubic (BCC) lattice of the micelle crystal. Through this work, we demonstrate the feasibility of this templating approach and also provide design criteria for developing structured thermo-reversible nanocomposites.

Keywords: Copolymer; Nanoparticle; Template; Cubic crystal; Neutron scattering

1. Introduction

Amphiphilic block-copolymers will form self-assembled structures when dispersed in solvents that are selective to some subset of the blocks [1]. The geometry and long range order of these structures depends on the chemistry of the polymer and the solution conditions among other controllable parameters [2–4]. Long range order in these systems occurs when the number of micellar aggregates (spherical, cylindrical or planar) exceeds the crystallization volume fraction. The repulsion between monodisperse spherical micelles drives the formation cubic phases (face-centered cubic or body-centered cubic) with order that persists over macroscopic length scales [1,3,5–9]. Since the observation of these phases, they have been considered for use as templates to impart order to materials that lack this ability to self-associate and organize. Examples of methods to template discrete and continuous structures have been described [10,11]. This contribution focuses on the organization of discrete nanoparticles in thermoreversible block-copolymer cubic crystals, an approach that has not been utilized in the past.

Block-copolymer mesophases in the presence of dispersed additives lead to composite systems that are used in a variety of fields including photonics [12], catalysis [13], bio-separations [9,14,15] and drug delivery [16]. In all of these applications, the internal structure of the materials at the nanometer scale plays a key role. For instance, the optical properties of block-copolymer composites containing templated gold nanoparticles are strongly influenced by changes in the interparticle distance [12]. Proximity effects, that could impact data storage applications, have also been observed in arrays of magnetic nanoparticles [17]. It is important that these effects, due to collective interactions,

* Corresponding author.
E-mail address: lwalker@andrew.cmu.edu (L.M. Walker).

0927-7757/$ – see front matter © 2006 Elsevier B.V. All rights reserved.
doi:10.1016/j.colsurfa.2006.08.002

are accurately controlled since they define the desired material properties.

Although examples of particle templating in block-copolymer mesophases are found in the literature [10], there is a lack of systematic work devoted to understanding the influence of experimentally controllable parameters on the particle array and on the polymer template itself. The reason for this gap in understanding is that most examples of successful templating have been based on the synthesis of the templated materials inside the ordered matrix. This restricts the systematic evaluation of the effect that variables such as relative size and relative concentration have on templating. These difficulties are in part due to variability between samples and because the synthesized phase will be thermodynamically driven to form stable structures. Additionally, the synthesis of particles inside the ordered phase severely reduces the applicability of templating to a handful of systems. A templating method that would be better suited for these studies and also expand its applicability is the dispersion of previously synthesized particles into the structured matrix. However, this type of templating is usually prevented by the large viscosity of the structured materials and the surface incompatibility of the particles with the polymers. Recently, we have shown that these problems can be circumvented by the use of thermo-reversible block copolymers and hydrophilic colloids [18,19].

Gels of polyethylene oxide (PEO) and polypropylene oxide (PPO) block copolymers, commercially known as Pluronic® or Poloxamer®, have been extensively studied over the past decade [3,6,8,9,20]. Both blocks of these copolymers are water soluble at low temperatures (<5 °C) and concentrated fluid dispersions are easily created. When the temperature is raised to values near room temperature the middle PPO block becomes increasingly dehydrated and the polymers self-associate into micellar aggregates. At large polymer concentrations, the spherical micelles pack into micelle cubic crystals and the viscosity of the samples increases by over four orders of magnitude. This transition is fully reversible on repeated heating and cooling. Pluronic® F127 is known to only form cubic structures of spherical micelles with a solid PPO core and a hydrated PEO corona [3]. We use this model system in our work because its solution behavior has been characterized extensively [3,6,8,9].

The thermo-reversible ordering behavior of these polymers and their water solubility make them ideal template materials for the incorporation of pre-made particle additives of nanometer size. We have used these templates to incorporate silica and gold nanoparticles as well as globular proteins [18]. The particles are incorporated at low temperatures while the matrix viscosity is low and the block copolymer phase is disordered. Repulsive forces between the nanoparticles are crucial to achieve a stable dispersion in this concentrated polymer solution. The temperature is then raised and the ordered cubic gel is formed around the dispersed particles. The particles remain trapped in the interstitial cavities of the cubic crystal and form an ordered array because these cavities also follow the crystal lattice. However, the order of the templated particles is less than that of the micelle crystal because there is significant freedom for translational motion inside the cavities and because defects (vacancies, overloaded cavities) are expected to occur. The crystal structure of these nanocomposites is expected to be analogous to the NaCl crystal. This crystal structure consists of an FCC crystal of smaller atoms (particles) intercalated in an FCC crystal of larger atoms (micelles). Although the stability of this phase in binary hard sphere mixtures has been predicted by simulations and theory, [21,22] it was only recently observed experimentally in colloidal systems [23,24]. Although other binary crystal superlattices (ZnS and CsCl) could also occur, the theory of hard-sphere mixtures predicts a higher stability for the NaCl superlattice [21].

We have observed that this templating method is quite general and can be applied to many particle systems as long as they can be initially dispersed in the concentrated polymer solution. Osmotic stresses in concentrated polymer solutions can be significant and electrostatic and/or hydration repulsive forces are essential to maintain particle stability.

In this study, we focus on the dispersion of nanosized and relatively monodisperse silica particles (Ludox®) because their interaction with the block-copolymers has been previously studied [25,26]. A stable NaCl phase is predicted in hard sphere mixtures for size ratios (small/large) $0.20 < \alpha < 0.42$ [21,22]. The size ratios of the particles used in this study are $\alpha \approx 0.3$ and $\alpha \approx 1.0$. Therefore, the small silica particles (Ludox® SM) are in the correct range to be well templated in the interstitial cavities of the cubic crystals while the large silica falls outside this range. We use this system as a model to evaluate the influence of various controllable parameters on the nanocomposite structure. We have already reported on the influence of these variables on the mechanical properties of these new materials [19]. In this contribution, we present neutron scattering experiments that support the structural picture and the results that were previously presented [18,19]. The use of block-copolymer cubic crystals in drug and protein delivery [27] and in bio-separations [9,14] motivates the need for fundamental understanding of these systems in the presence of particles.

2. Experimental

2.1. Materials and sample preparation

Ludox® silica particles (Ludox® SM-30 and Ludox® TM-50) are obtained from Grace Davidson (Columbia, MD) and used as received. These silica particles are dispersed in water at a pH near 10. At this pH the particles have a zeta-potential of about −70 mV and remain stable for long periods of time.[28] Ludox® SM is reported by the manufacturer to have a particle diameter of 7 nm while Ludox® TM has a diameter of 22 nm. However, these materials have some size polydispersity so the reported dimensions are average values. Pluronic® F127 is obtained from BASF (Mount Olive, NJ) and is also used as received. The reported chemical structure for this Pluronic® material is $PEO_{99}PPO_{69}PEO_{99}$ [9]. All polymer and particle dilutions are performed using de-ionized water (18 MΩ) or 99.8% deuterium oxide D_2O that is obtained from Aldrich Chemical Company (Milwaukee, WI).

The F127 powder is first allowed to dissolve in a 35 wt.% stock solution over several days in an ice bath. Polymer stock

solutions are dissolved in H_2O or in D_2O to prepare samples with variable D_2O/H_2O ratios. The polymer and silica concentration in the samples is limited by the initial concentration of the silica stock solutions. Concentration and re-dispersion of the silica stock is avoided as it leads to irreversible particle flocculation.

A strict order of addition is followed to minimize the particle destabilization that occurs when large concentration gradients are formed during mixing. The particle stock solution is first diluted and mixed with the necessary amounts of H_2O and D_2O. The required amount of a 35 wt.% stock solution of F127 (in H_2O or D_2O) is then added at low temperatures so that the solution is fluid. The samples are then vigorously shaken and allowed to equilibrate in an ice bath. The resulting samples are fluid at low temperatures and are as transparent as aqueous silica suspensions at corresponding concentrations. In a few cases (largest silica and polymer concentrations), a small amount of flocculated silica is observed for samples containing high polymer (30 w%) and silica concentration (above 8 w% silica). In these cases, the sample preparation is repeated to minimize this effect and centrifugation at low temperatures is used to separate any remaining aggregates. Intentional flocculation of the dispersed particles, through the addition of salt, shows that the amount of flocculated silica that is removed by centrifugation is a negligible fraction of the total silica content.

2.2. Small-angle neutron scattering

Neutron scattering experiments are carried out at the NIST Center for Neutron Research (NCNR) in Gaithersburg, MD. The data are collected using the 30 m SANS instruments NG3 and NG7. A neutron wavelength of 6 Å with a spread $\Delta\lambda/\lambda$ of 0.15 is used at several detector distances (1.1, 4.5 and 12 or 13.1 m) to gather the scattering profiles. While not all detector distances are used for all the samples, an overall Q range of $0.0035 < Q < 0.4$ Å^{-1} is accessible. Samples are loaded in quartz cells with a 1 mm path length. The temperature is controlled to within ± 1 °C in a cell block heated by circulating ethylene glycol. The scattering profiles are appropriately reduced to an absolute scale by referencing to the open beam neutron flux. The background incoherent scattering, mostly due to hydrogen atoms in the solvent and the polymer, is subtracted after measuring at high wavevector values ($Q > 0.2$ Å^{-1}). A Couette shear cell specially designed for SANS experiments is used to shear align the samples. A gap of 0.5 mm was used in the radial geometry so that the total scattering sample thickness is also 1 mm. The design and operation of the shear cell has been described elsewhere [29].

3. Results

To interpret the scattering data from composite materials, the contributions from individual components was first characterized. Fig. 1 shows the circularly averaged scattering profiles for the silica particles in water. A polydisperse sphere model is used to fit the data. This simple model successfully represents the Ludox® TM particles with an average diameter of 24 nm and a polydispersity index of 0.2 [30]. However, the model is unable to reproduce the scattering data from the smaller silica (Ludox® SM). Adequate modeling results are obtained by using two separate polydisperse modes with average diameters of 16 (20 vol.%) and 6 nm (80 vol.%). This bi-disperse model successfully reproduces the data and the particle size are consistent with that reported by the manufacturer. Since the particles have substantial polydispersity, there is some uncertainty in the average particle size and polydispersity that is obtained from SANS for both types of particles. Therefore, the nominal particle sizes of 7 and 22 nm (obtained from the manufacturer) are used to identify samples here for consistency in comparison to other published work. The ramifications of this polydispersity are discussed later. From the data, it is apparent that larger particles are significantly more monodisperse than the smaller particle size. The existence of two particle populations in the 7 nm Ludox® SM is due either to the synthesis or to a decrease in particle stability and aggregate formation.

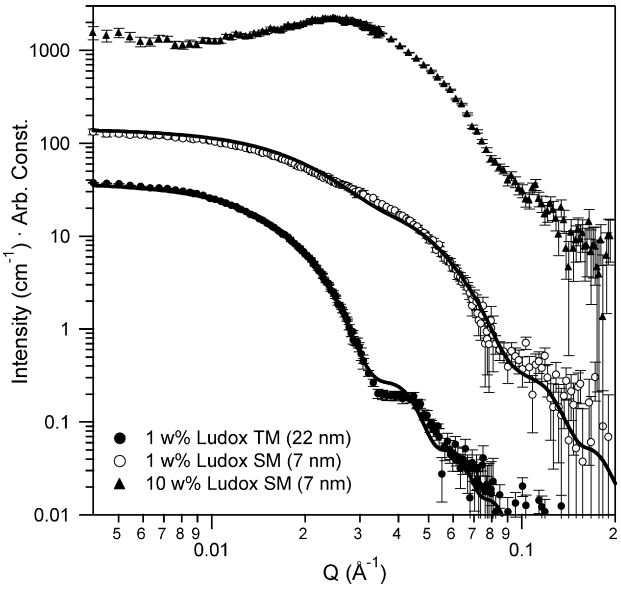

Fig. 1. Neutron scattering profiles for silica particles in 15% D_2O. The data for the 7 nm particles are shifted vertically for clarity. Straight lines represent a monomodal polydisperse sphere form factor for Ludox® TM and a bimodal distribution for Ludox® SM.

The scattering from a concentrated dispersion of particles (10 wt.%) is also shown in Fig. 1. Particle–particle interactions are apparent from the broad peak near 0.025 Å^{-1}. The peak intensity is found to decrease with the addition of salt (20 mM NaCl). At this silica concentration, the particles are about 10 nm apart and the Debye screening length ($1/\kappa$) is on the order of a nanometer. This salt dependence indicates that this interaction peak is in part due to electrostatic repulsion between the negatively charged particles. Due to the particle polydispersity, the form factors for the silica particles are measured at 1 wt.% in D_2O rather than calculated.

The circularly averaged scattering profiles for the neat polymer matrix in the gel state are shown in Fig. 2 for various polymer concentrations. The small-angle scattering of the neat micelle crystals has been characterized extensively with neutrons and X-rays [3,5,6,8,9]. Samples at concentrations lower

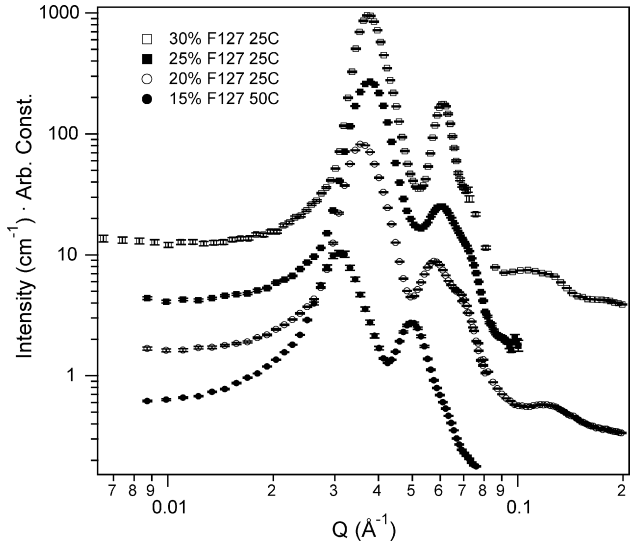

Fig. 2. Neutron scattering profiles for Pluronic® F127 cubic gel samples in D_2O at various polymer concentrations and temperatures. The 15%, 25% and 30% F127 curves are shifted vertically for clarity.

than 15 wt.% do not show reversible gelation behavior and therefore are not suitable as polymer templates. For concentrations above 15 wt.%, the profiles show two peaks and a broad shoulder that are characteristic of SANS profiles of face centered cubic (FCC) crystals [9]. The position of the first peak shifts to lower Q values as the concentration of polymer is lowered. The shift in the peak position indicates that the unit cell size of the cubic crystal is larger for the lower polymer concentrations. Wu et al. performed SANS and SAXS experiments on the same Pluronic F127 samples and showed that the cubic structure of the crystals was indeed FCC [9] and not body centered cubic (BCC) as previously thought [8]. Neutron scattering experiments have smearing effects that are larger than those in X-ray experiments and result in the combination of adjacent peaks into a single broad peaks. These effects led to a few conflicting results in the literature and caused some difficulties in the structural interpretation of the scattering patterns. Here, we will base our analysis on the conclusion that the cubic phase formed is FCC; the result reached through a combination of SANS and SAXS [9].

Once the gel structure has been identified as FCC, it is possible to obtain lattice parameters from the peak positions. The first SANS peak in the data are a combination of the diffraction from the (1 1 1) and the (2 0 0) planes [31]. The position of the first SANS peak can be approximated as the (1 1 1) peak position because it dominates the intensity. The second peak in the SANS patterns is due to the (2 2 0) diffraction plane. Therefore, the unit cell size (a) and the hard sphere diameter (D_{HS}) are estimated using the first peak position (Q_{max}) using,

$$a = \frac{2\pi}{Q_{max}}\sqrt{h^2+k^2+l^2} = \frac{2\pi}{Q_{max}}\sqrt{3} \quad (1)$$

$$D_{HS} = \frac{\pi\sqrt{6}}{Q_{max}}. \quad (2)$$

From Eqs. (1) and (2) and the data shown in Fig. 2 we estimate D_{HS}, the distance between adjacent micelle centers, for the crystals as a function of concentration. This value ranges from 24.9 nm at 15 wt.% F127 to 19.7 nm at 35 wt.%. Good agreement (<1 nm difference) is found when the second SANS peak is used to calculate this distance, which further validates the FCC model. Therefore, as the concentration of polymer is increased, the micelles are pushed closer together and the dimensions of the interstitial cavities are reduced. Additionally, the larger overall polymer concentration also increases the PEO segment density in the continuous phase and tightens the space around templated particles.

Table 1
Ratio of the particle diameter to the estimated octahedral interstitial site dimension (D/OIS) for 7 nm (Ludox® SM) and 22 nm (Ludox® TM) particles

F127 wt.%	D/OIS	
	Ludox® SM	Ludox® TM
15	0.68	2.13
25	0.83	2.61
35	0.86	2.69

The largest interstitial dimension, the diameter of the largest sphere that will fit into an interstitial cavity, can be estimated geometrically from the lattice parameter. For an FCC crystal, this dimension is equal to 41.4% of the size of the micelles for the octahedral sites and 22.5% of the micelle for the tetrahedral sites. Naturally, this value is only an estimate of the real dimension of the interstitial cavity. The true cavity size will be different because micelles are not true hard-spheres and there is significant interdigitation between the segments of the corona. Therefore, the sizes of the interstitial cavity mentioned above provide an upper limit estimate on the space available to a templated particle. However, these structural dimensions are useful to approximate the relative dimension of templated particles to the interstitial sites. Table 1 compares the size of silica particles to the octahedral sites (OIS).

The generalized scattering equation for a three component system is given by:

$$I(Q) = (\rho_1-\rho_s)^2 I_{11}(Q) + (\rho_2-\rho_s)^2 I_{22}(Q) + 2(\rho_1-\rho_s)(\rho_2-\rho_s)I_{12}(Q). \quad (3)$$

In Eq. (3), ρ_1, ρ_2 and ρ_s are the scattering length densities (SLD) of component 1, component 2 and the solvent, respectively. $I_{11}(Q)$ and $I_{22}(Q)$ represent the scattering contributions from the pure components and $I_{12}(Q)$ is a term due to cross correlations between the two dispersed materials. One useful property of neutrons is the different interaction with atomic isotopes. This allows use of isotope solvent mixtures to change the SLD of solvents without significantly altering the chemistry and interactions in the samples. In a contrast matching experiment, the SLD of the solvent is matched to that of one component so that the scattering signal from the second component is recovered,

$$I(Q) = (\rho_2-\rho_s)^2 I_{22}(Q) \quad \text{for } \rho_s = \rho_1. \quad (4)$$

The SLD of the pure components is calculated from the atomic composition and the density of the materials [32]. The contrast matching solvent compositions are calculated and it is found

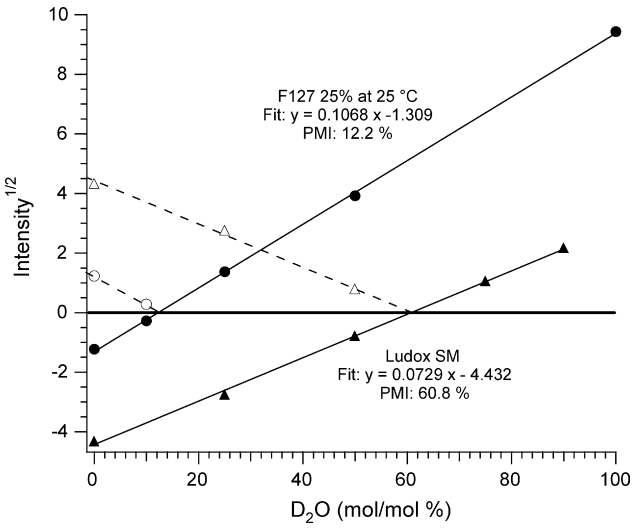

Fig. 3. Experimental determination of the point of minimum intensity (PMI) for the silica particles and the F127 block copolymer. Open symbols represent the measured intensities before multiplication by −1 to perform the linear fit (solid lines).

that the silica particles are matched with a solvent composition containing 58% D_2O (mol/mol). Although it is not possible to perfectly match the F127 chains because the two blocks have different scattering length densities ($SLD_{PEO} = 0.572 \times 10^{-6}$ Å^{-2} and $SLD_{PPO} = 0.347 \times 10^{-6}$ Å^{-2}) [4] a point of minimum intensity (PMI) can be defined. For F127 the PMI is calculated using the average chemical structure of the chain and it is calculated to be at a solvent composition of 15% D_2O (mol/mol). The SLD of PEO and PPO are so similar that the scattering intensity at the PMI is negligible and the whole polymer chain can be regarded as being matched by the solvent.

The values of the PMI for the polymer and the contrast matching point for the silica were also determined experimentally. Fig. 3 shows the square root of the maximum intensity, $I(Q \rightarrow 0)$ for the silica and $I(Q_{max})$ for the Pluronic® crystal, as a function of molar percent of D_2O in the solvent. The experimental values for the PMI are determined to be 60.8% for the silica and 12.2% for the polymer. The 3% discrepancy between the values used in sample preparation (calculated values) and the true values does not result in significant error because the residual intensity is always significantly lower than the signal of interest (see below). The discrepancy in the PMI value of the polymer is likely due to larger contribution of the solid micelle core (PPO) to the total intensity. In the case of the silica, the discrepancy could be due to unaccounted impurities in the particles or to differences in the nanoparticle density with respect to bulk silica (2.2 g/mL). All measurements, with the exception of the sheared samples, are performed using the calculated values of the PMI. Key experiments, including shear-alignment, were verified using the measured values of PMI which are more accurate.

The two-dimensional scattering profiles for a gelled sample containing 25 wt.% F127 in the matrix and 3 wt.% 7 nm silica particles are shown in Fig. 4. The scattering signal due to the particles (polymer matched) is shown in the top (A and B) while the scattering from the polymer micelles (silica matched) is shown in the bottom profiles (C and D). The scattering data were collected at rest (A and C) and under an applied shear rate of 10 s^{-1} (B and D). The samples were loaded as a fluid at low temperature and then heated to 25 °C in the shear cell. Therefore, the micelle crystal initially forms with no preferential orientation and the scattering is consistent with that of a polycrystalline powder. Diffraction in a powder sample is observed as concentric rings like those seen in Fig. 4C. In this state, the polymer template shows clear rings and the dispersed particles also show an isotropic scattering pattern. When the samples are sheared at a rate of 10 s^{-1} (B and D), macroscopic orientation of the sample results in the formation of discrete peaks. This alignment results in a hexagonally symmetric pattern that develops at the appropriate wave vector value ($Q = 0.035$ Å^{-1}) in the polymer scattering. The same symmetry is also seen in the templated silica particles. As expected, this six-fold symmetry appears at a similar wavevector ($Q = 0.035$ Å^{-1}) in both the polymer micelles and the disperse silica. These results verify that the particles are indeed templated by the micellar cubic phase and the spacing is consistent with the picture of nanoparticles partitioned to the interstitial spaces in the block-copolymer cubic phase. The structure of the nanocomposite is analogous to that of a NaCl crystal with the silica particles occupying the octahedral sites between the micelles.

When FCC cubic crystals are sheared, they orient with the (1 1 1) plane parallel to the wall of the shear cell. In this conformation, the crystal can be described by a set of hexagonally close packed particle layers that are stacked along the shear gradient direction. The scattering from the flowing crystals is consistent with a model of sliding hexagonal layers [33]. For well templated nanocomposites, the crystal orientation and the lattice spacing of the micelle crystal and the templated particles is the same. Therefore, the scattering from both phases presents a hexagonal pattern with the same orientation and Q position. The hexagonal pattern in the silica scattering (Fig. 4B) is blurred due to the form factors and because the lattice is significantly more defect ridden than that of the polymer template. Still, the formation of a hexagonal pattern is evident. A more detailed description of shear alignment in these nanocomposites will be provided in a future article. Here, we perform an extensive evaluation of the design parameters using nanocomposite samples at rest. To effectively probe a number of variables, samples are studied only at rest, without the alignment provided by shear, therefore the samples are in powder (polycrystalline) form and the isotropic scattering patterns are circularly averaged to assess the quality of the templating.

Fig. 5 shows the circularly averaged scattering profiles for a sample containing 20 wt.% F127 and 4 wt.% 7 nm silica with the solvent "matched" to the silica particles (58% D_2O). At low temperatures, the samples are fluid because the polymer chains are hydrated and behave like random coils. As the temperature is raised to 11 °C, micelles begin to form and this is reflected in the changing scattering profile. Although there is no micelle interaction peak, the scattering profile and the rheology [19] indicate the onset of micellization. Unlike small molecule surfactants these systems do not have a sharp micellization transitions and there is a small region of coexistence between micelles and hydrated coils.

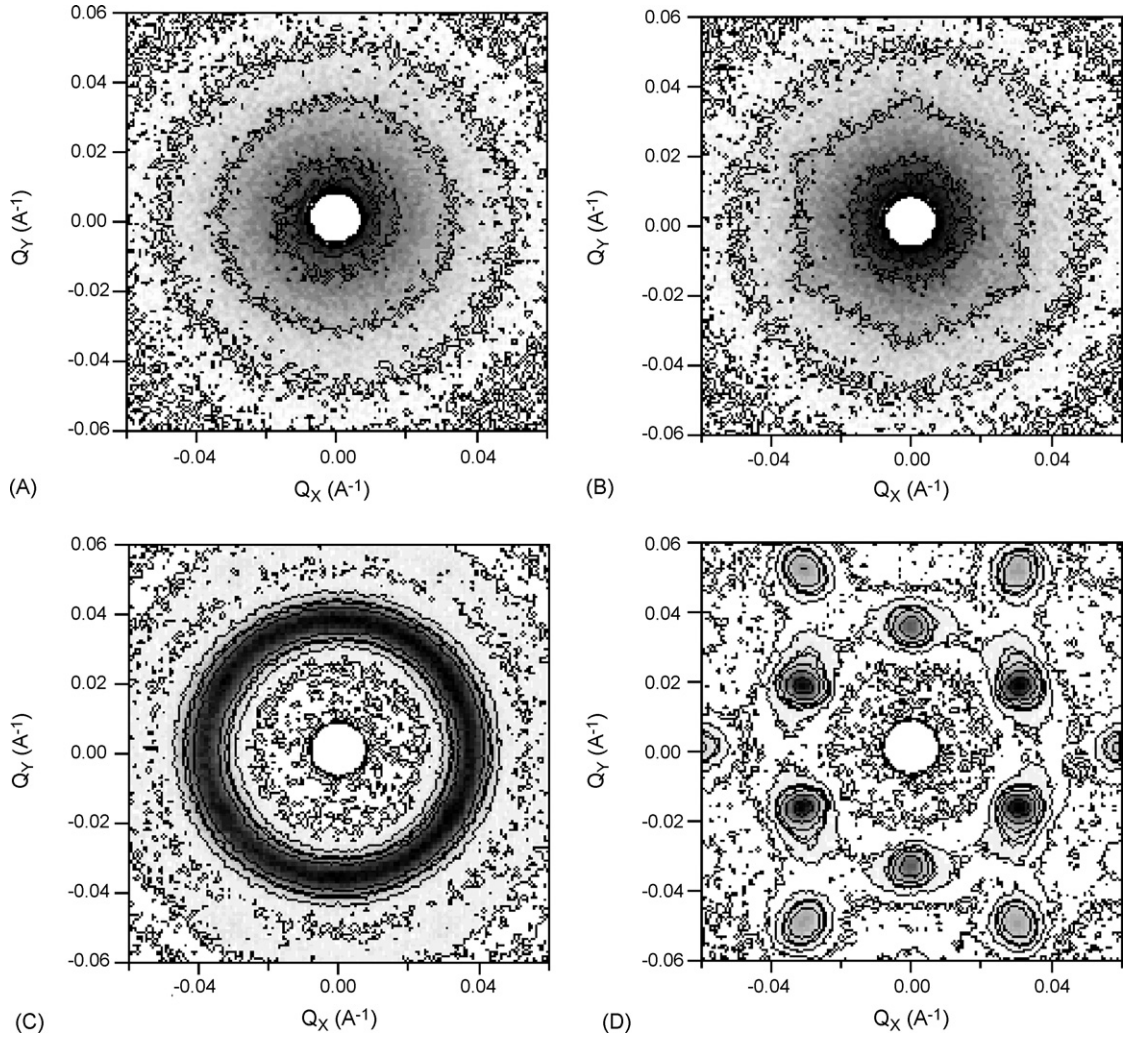

Fig. 4. Two-dimensional scattering profiles for a nanocomposite sample containing 25 wt.% Pluronic F127 in the matrix and 3 wt.% 7 nm silica particles. Top profiles represent the scattering from the silica particles (12% D_2O) at 0 (A) and 10 s^{-1} (B). Bottom profiles represent the scattering from the polymer micelles (61% D_2O) at 0 (C) and 10 s^{-1} (D). The intensity is doubled between two contour lines.

At 35 °C micelles form and pack into a cubic structure. The structural transition of the pure block copolymers [5,7,8] and the nanocomposites [19] has been previously studied with rheology. Although these phases are commonly called gels, in reality they are viscoelastic materials with long relaxation times [34]. The scattering from the cubic crystal in the presence of particles is similar to that of the neat polymer matrix but there is an increased scattering at low Q and the diffraction peaks are somewhat broadened. When the temperature is increased further, the scattering at low Q increases and the peaks are broadened further. The second diffraction peak is also observed to decrease in magnitude with increasing temperature. The residual scattering intensity from the particles is also shown in Fig. 5. While the residual scattering shows some Q dependence, the intensity is so low that it is a negligible contribution to the scattering from the nanocomposites.

The scattering arising from the silica particles (solvent containing 15% D_2O) is shown in Fig. 6 as a function of temperature. This sample also contains 4 wt.% of 7 nm silica particles and 20 wt.% F127 in the continuous matrix. At low temperatures the scattering profile for the particles is similar to the scattering from silica particles in water (Fig. 1). This shows that particles are primarily randomly dispersed in the solvent. When the temperature is increased, and the polymer forms an ordered matrix, the scattering from the particles is significantly altered. A dip in the profile is observed at the Q position corresponding to the peaks of the polymer cubic template ($Q = 0.035$ Å^{-1}). The residual scattering intensity from the polymer is also included in the plot. In this case, the residual intensity is even lower than that shown in Fig. 5 and the difference in signal intensity (silica) to residual intensity (polymer) is close to two orders of magnitude.

The scattering from solid spherical particles is often separated into two terms arising from the particle shape $P(Q)$ and the interparticle correlations $S(Q)$,

$$I(Q) \approx N(\rho - \rho_s)^2 S(Q) P(Q) + \text{bkg.} \quad (5)$$

The form factor $P(Q)$ is measured directly at low particle concentrations (Fig. 1). The structure factor $S(Q)$ is then obtained from samples with interacting particles by normalizing the data

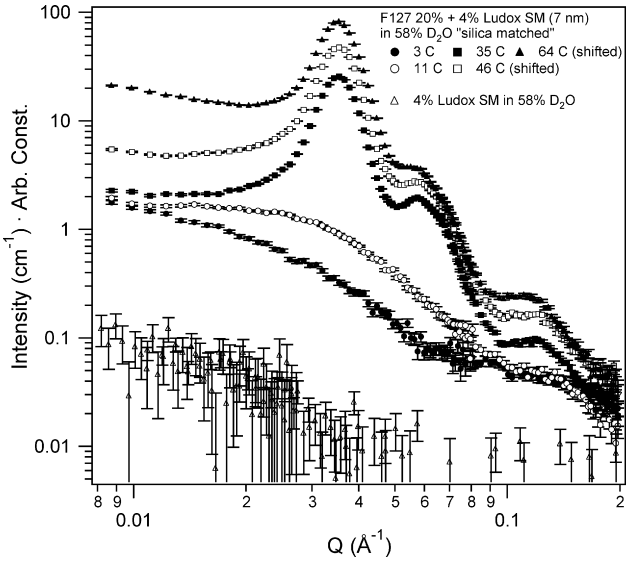

Fig. 5. Temperature dependence of quiescent samples containing 20 w% F127 and 4 w% 7 nm silica particles. The scattering length density of the solvent (58% D_2O) is matched to that of the silica particles. The curves for the 64 °C and 46 °C are shifted vertically for clarity.

with $P(Q)$ and the different concentrations. We use this simple approach to extract structural information about the silica nanoparticles dispersed in the structured Pluronic® gel. $S(Q)$ approaches unity for randomly dispersed particles in dilute conditions.

Fig. 7 shows the structure factor for various samples at different temperatures corresponding to the fluid state (3 °C) and the gel state ($T > 25$ °C). The structure factor for the sample containing 7 nm particles in a matrix of 20 wt.% F127 (Fig. 7A) approaches unity at 3 °C because the micelle crystal has not formed. When the temperature is increased to 35 °C, a broad peak is formed near $Q = 0.03$ Å^{-1} and the value at low Q

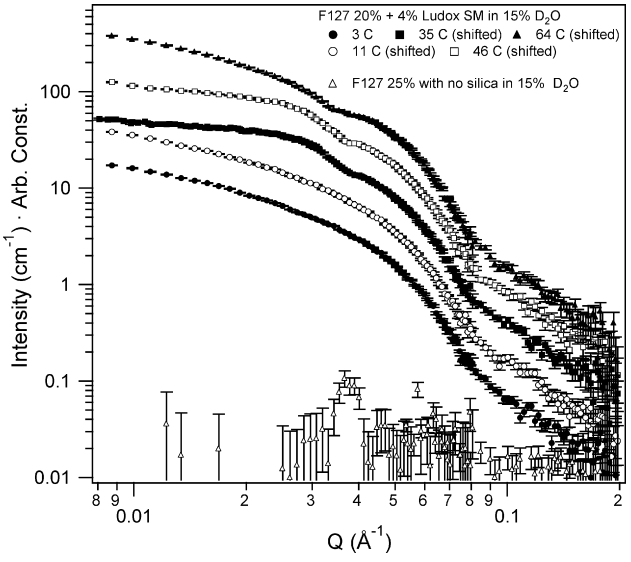

Fig. 6. Temperature dependence of quiescent samples containing 20 wt.% F127 and 4 wt.% 7 nm silica particles. The scattering length density of the solvent (15% D_2O) is matched to that of the polymer. The curves from data at 11, 35, 46 and 64 °C are shifted vertically for clarity.

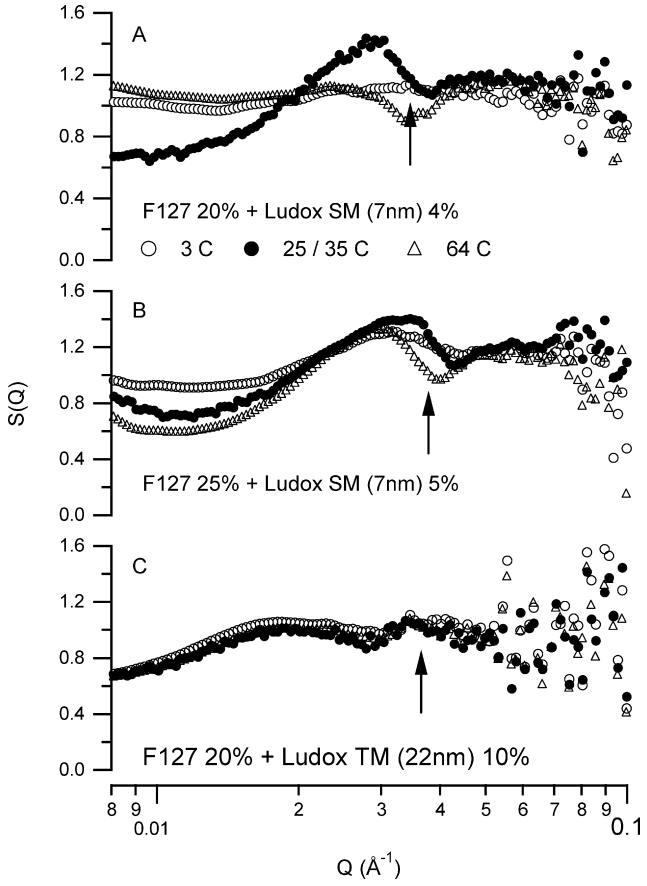

Fig. 7. Structure factors for the silica particle correlations as a function of temperature for 7 nm particles in a matrix of (A) 20% F127 and (B) 25% F127 and (C) 22 nm silica in a matrix of 20% F127 at 3 C (◯) 25 or 35 °C (●) and 64 °C (△).

decreases. At a larger temperature, the peak in the structure factor decreases again. When the matrix contains 25 w% F127 (Fig. 7B) an interaction peak is observed at all temperatures. This indicates that even at 3 °C, where the samples are still fluid, there are some spatial correlations between the silica particles. When the temperature of this sample is increased to 25 °C, we observe an increase in the $S(Q)$ peak near $Q = 0.035$ Å^{-1} and a lowering of the values at low Q. As the temperature of this sample is raised to 64 °C the intensity of the broad peak decreases and it is shifted to lower Q. The sample that contains the 22 nm silica particles (Fig. 7C) also shows structure factor effects (especially at low Q). However, these features are much shallower than those on the samples containing the smaller silica. More importantly, the features are independent of temperature indicating that the particles are not templated by the matrix because they are larger than the interstitial cavities. The fact that the particle–particle structure factors are the same in the fluid (3 °C) and gelled states (25 °C) suggest that this is due to interparticle interactions that already exist in the fluid state and that gelation only causes the kinetic trapping of this average particle distribution.

The scattering from the 7 nm silica particles in the nanocomposites is also collected as a function of particle concentration. Previous rheological experiments show that the silica concentration significantly affects the mechanical and optical properties

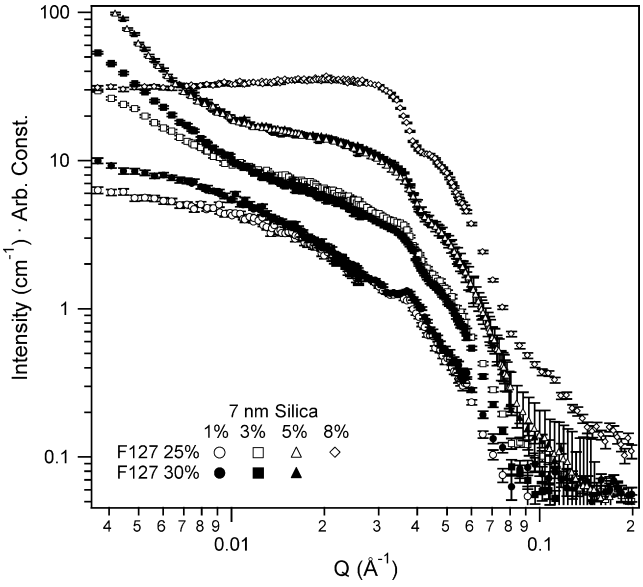

Fig. 8. Scattering profiles for quiescent samples containing variable amounts of 7 nm silica and F127 at 25 °C. The solvent is matched to the polymer micelles (D_2O 15%). The curves from samples with 3%, 5% and 8% silica are shifted vertically for clarity.

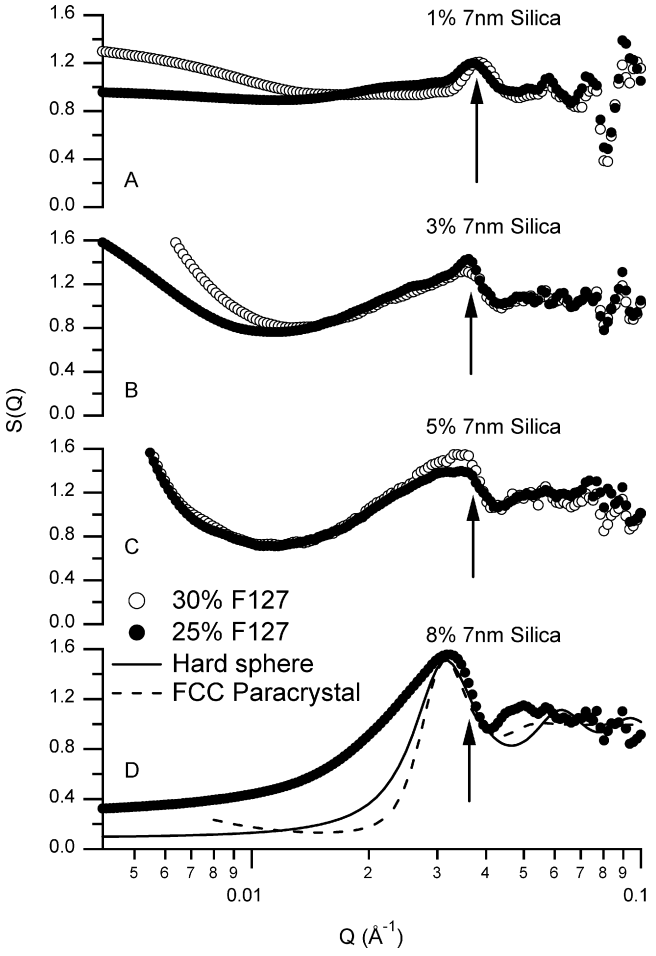

Fig. 9. Structure factors of quiescent samples as a function of 7 nm silica concentration in a matrix of 25% F127 (●) and 30% F127. A hard sphere (solid line) and a paracrystal (dashed line) models are shown for the sample containing 8% silica. Arrows point to the relative Q position of the first peak in the scattering from the polymer micelles (25 wt.% F127).

of the nanocomposites [19]. Although the SANS data indicates that the 7 nm silica particles (Ludox SM) have two particle size modes (6 nm and 16 nm), the structure and mechanical properties of the nanocomposite samples are dominated by the smaller particle fraction. This is because the small particles exist in a much larger fraction (96% by number) and because large particles have been shown to have significantly less influence on the structure and mechanical properties of these samples [19]. Fig. 8 shows the scattering profiles for nanocomposites containing variable concentrations of 7 nm silica particles with two different polymer concentrations in the matrix (25 wt.% and 30 wt.%) at 25 °C. The templating effect of the polymer is evident as the scattering is compared to that shown in Fig. 1 for the particles in water. At low particle concentrations, the scattering is similar to that of Fig. 1 with the exception of the peak that occurs at $Q = 0.037$ Å^{-1}. The scattering at larger silica loadings (3–8 wt.%) is significantly different from the scattering in dilute solution (Fig. 1). The main differences are an increased scattering at low Q and the deformation of the profile near $Q = 0.035$ Å^{-1}. The increase in intensity at low Q values is evidence of phase separation and is discussed in detail in the following sections.

To gain insight into these changes, the structure factor for these samples in the gelled state is calculated and shown in Fig. 9 as a function of composition. The primary peak of the structure factors at low particle concentrations (Fig. 9A) occurs at the same Q value of the corresponding cubic crystal template (arrows). This is a clear indication of effective particle templating. At this silica concentration (1 wt.%) the ratio of particles to octahedral interstitial cavities is low (0.15 particle/site). It is important to note that this occupancy ratio is calculated for a homogeneous dispersion of nanoparticles. Phase separation into particle-rich and particle-poor phases will result in larger and lower local occupancy ratios that can have a significant effect on the scattering signal. No secondary peaks can be reliably obtained from the data due to the significant incoherent scattering at high Q. This lack of higher order peaks complicates the identification of the crystal lattice of the templated particles. Although the possibility that the nanocomposites follow other crystal structures (CsCl, ZnS) cannot be excluded based on the powder scattering, the scattering peaks in the shear-aligned runs are consistent with a crystal lattice that is analogous to the NaCl structure.

The structure factor at 3 wt.% silica (Fig. 9B), corresponding to 0.52 particles/site, shows a diffraction peak that is larger and sharper than that of Fig. 9A. The peak also shows a complex functionality towards low Q (the peak is asymmetrical). The increased amplitude at low Q also indicates the formation of large domains with different scattering contrast. This increase develops at lower silica loadings for samples containing 30 wt.% F127 in the matrix. The samples containing 5 wt.% silica (0.95 particle/site) also show the formation of sharp peaks around $Q = 0.035$ Å^{-1} (Fig. 9C). At this silica concentration, the 25 wt.% and the 30 wt.% F127 samples show the same form of

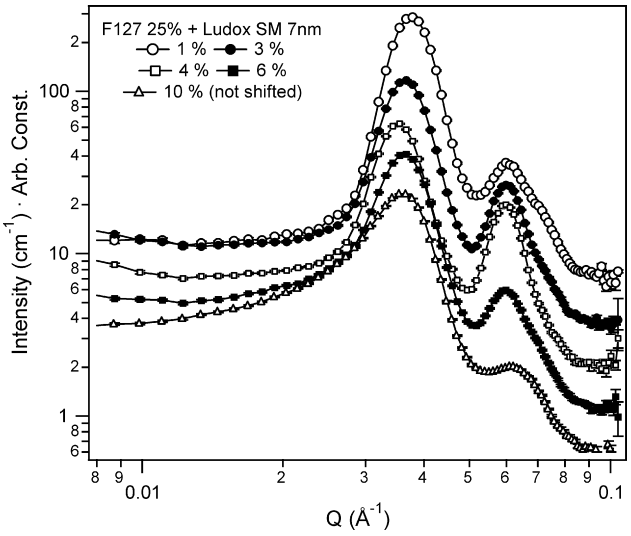

Fig. 10. Neutron scattering profiles for quiescent samples containing 7 nm silica particles. The samples contain 58% D_2O and the scattering signal is due to the polymer matrix. All curves, with the exception of the 10% silica sample, are shifted vertically for clarity.

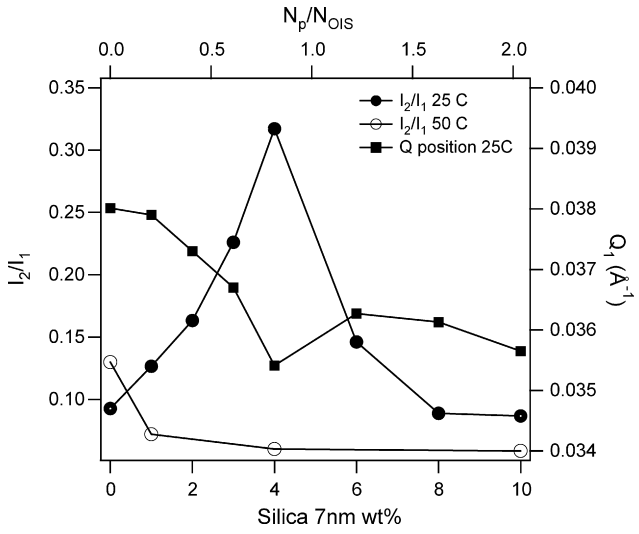

Fig. 11. Ratio of the intensity of the second diffraction peak to the first (I_2/I_1) at 25 °C (●) and 50 °C (◯) for data series shown in Fig. 9. The position of the first diffraction peak (Q_1) is also shown for the samples at 25 °C (■). Top axis shows the calculated relative number of particles to the octahedral interstitial sites (N_p/N_{OIS}).

increase at low Q. A sample containing 8 wt.% silica (1.53 particle/site) in a 25 wt.% F127 matrix is also analyzed and shows a significantly different structure factor (Fig. 9D). This sample shows a larger but significantly broader peak and a flat low Q scattering. The low Q functionality at high silica concentration indicates that the nanoparticle distribution is more homogeneous throughout the sample. The structure factor peak of this sample is more intense than those of lower silica concentrations. However, the peak is significantly broader and the Q position deviates from the position of the peak in the scattering of the polymer micelles. This suggests a lower degree of templating order.

The scattering patterns resulting from the polymer matrix (58% D_2O) of nanocomposites containing variable amounts of 7 nm silica nanoparticles is shown in Fig. 10. The patterns are characteristic of Pluronic® cubic crystals but they contain features that develop with the addition of silica. The most evident change in the scattering patterns is a variation in the relative intensity of the secondary peak with respect to the primary peak as the concentration of silica is increased. When silica is added up to 4 wt.% the intensity of the second peak increases relative to the first peak. As the concentration of silica is increased further, there is a decrease in the relative intensity of the second peak.

The ratio of the second peak intensity to that of the first peak is shown in Fig. 11 and the non-monotonic change becomes more evident. The top axis in Fig. 11 shows the relative number of particles to octahedral interstitial cavities calculated with the nominal particle diameter (7 nm) and the scattering from the polymer templates. Interestingly, the largest changes appear to occur as the concentration of particles is changed around the estimated value of 1 particle per site. Fig. 11 also shows the position of the primary peak with the addition of silica. This value also shows a non-monotonic change around silica concentration of 4 wt.%. At this silica concentration the shift in Q is equivalent to an increase of 1.3 nm in the nearest neighbor distance between micelles (D_{nn}). Fig. 11 also includes the ratio of the peaks for samples at 50 °C and shows that, at this temperature, the values are smaller than those at 25 °C for all silica concentrations.

4. Discussion

4.1. Nanoparticle templating

The feasibility of using self-assembled micelle cubic crystals to template nanoparticles is demonstrated by the scattering profiles arising from the silica nanoparticles. The scattering data and the interaction between the silica and the PEO segments of the Pluronic® block copolymer suggest that the particles are located in the continuous PEO–water matrix. The PEO blocks of the Pluronic® chains have been found to absorb in small amounts to silica surfaces (<0.4 mg/m^2) while the PPO segment adsorption is even less [25,26]. Additionally, we do not believe that the particles are located in the core of the micelles because the magnitude of the peaks in the structure factors would be significantly larger as the nanoparticle correlations would be similar to those of the micelle crystal template. The scattering profiles shown for the silica phase compared to that of the micelle phase indicate that there is still significant disorder and less than perfect organization.

In an attempt to quantify the nanoparticle order we attempted to fit the measured structure factors (Fig. 9) to a paracrystal model [35,36] and to a hard sphere fluid model [37]. The paracrystal model starts from a perfect crystal lattice and provides a variable degree of distortion (g parameter) in the "atom" positions in the crystal. This can simulate the distortion that is caused by particle motion in the crystal, lattice defects and smearing observed in the experimental data. When the lattice (FCC, BCC or SC) is known, the two adjustable parameters in this model are the unit cell dimension and the distortion parameter (g). The adjustable parameters in the hard-sphere model are

the effective volume fraction (volume fraction of hard spheres) and the effective hard sphere diameter.

The complex $S(Q)$ waveform at 1–5 w% could not be reproduced by either a hard sphere model or a cubic paracrystal model. Therefore, the interparticle structure of the silica in these nanocomposites is significantly more complex than that which is predicted from fluid (hard-sphere) or crystalline models (paracrystal). This suggests that the scattering in these samples can only be successfully modeled after the inclusion of more realistic complexities including particle-rich particle-poor phase separation, finite crystal domains and lattice defects. Although some of these effects can be included in the models, [35] the influences of other complex effects like particle polydispersity cannot be easily included.

These two models were also tested on the data at a large silica concentration. The model predictions are shown in Fig. 9D. For this sample, the low Q region of the structure factor could be successfully reproduced by a hard sphere model with an effective hard-sphere diameter $D_{HS} = 22.8$ nm and a volume fraction $\phi = 0.15$ but the model under-predicted the height of the peak. When the model was forced to reproduce the peak position and height ($D = 20.4$ nm, $\phi = 0.30$), the low Q scattering was underestimated and the high Q region was misrepresented. An FCC paracrystal model with nearest neighbor distance $D_{nn} = 24$ nm and distortion parameter $g = 0.26$ was also used to model the structure factors but did not result in acceptable reproduction of the data. Although the high Q oscillations were reproduced somewhat better than the hard-sphere model, the model fails at low Q. Therefore, the fluid and crystal models also fail in the limit of high silica concentrations and more realistic models are required to successfully reproduce the data.

The neutron scattering results are also consistent with the structural model that we previously proposed to explain their mechanical behavior [19]. At low concentrations of 7 nm silica particles, the samples were found to be mostly transparent and their temperature dependent mechanical properties are similar to those of the neat cubic crystal. At intermediate silica concentrations ($2 < \text{wt.\%} < 8$), the samples become increasingly turbid and the rheological properties change drastically with silica concentration. At large concentrations (>8 wt.%) the samples become transparent again and flow more easily. We postulated that this behavior is due to the changes in the ratio of dispersed particles to available interstitial cavities. At low particle loadings the crystal structure is only slightly perturbed and particles are well templated by the crystal. At intermediate silica loadings there is a phase separation between regions of crystal that are rich in particles and regions of neat micelle crystal. It is important to note that the measured scattering profiles include contributions from all the coexisting phases that contain the scattering components. This point is more important in the scattering profiles from the polymer crystal (silica matched) because the polymer is distributed nearly equally in both the particle-rich and the particle-poor regions. In the case of the silica scattering (polymer matched), the profiles are predominantly due to scattering from the particle-rich regions which contain most of the particles. For these samples, the low Q increase of the structure factor is related to the size and shape of the particle-rich domains. Experiments that probe the structure at lower values of Q, like USANS, are better suited to characterize this phase separation. At even larger silica loadings, the number of particles exceeds the number of available template sites and the structure is rich in defects. At this point the crystalline nature of the materials is lost and the structure resembles a kinetically hindered but locally disordered amorphous fluid phase.

This phase behavior is not due to polymer adsorption on particles because this amount is small in comparison to the total polymer concentration. Additionally, samples prepared with polyethylene oxide homopolymer of similar molecular weight do not show any phase separation in the same temperature and concentration range. In our rheological experiments, the appearance of a coexisting fluid phase also resulted in significant weakening of the nanocomposites [19].

The influence of particle concentration on the templating ability of the crystal is clearly observed in Fig. 9. At low particle loadings there is a strong correlation between the position of the silica structure factor peak and that of the polymer crystal (arrows). When the concentration is larger the correlation between the structure factor and the polymer peak is less and less. The increase of the magnitude in the structure factor peak is not necessarily due to increased ordering but to the larger volume fraction of particles. The agreement between the peak position of the polymer template scattering and the silica scattering is a better parameter to evaluate templating quality. The non-monotonic change (increase then decrease) of the low Q scattering intensity with the particle concentration is also a clear indication of the phase separation into regions that are rich in templated nanoparticles and regions that are poor. At the largest silica concentration, the structure factor becomes flat at low Q indicating that the sample is again homogeneous. The upturn at low Q also occurs first when the polymer concentration is larger. This suggests that the particle-poor particle-rich phase separation is due to the stress caused by lattice incompatibility and this is expected to be larger for more concentrated samples.

Improved nanoparticle templating is obtained at larger concentrations of polymer in the matrix. Fig. 9 shows that 25 wt.% and 30 wt.% F127 result in similar correlation peaks. However, in Fig. 7 we observe that the correlation peak from the sample containing 20 wt.% F127 deviates from the position of the peak in the scattering due to the micelles (arrow). The lower polymer concentrations in the matrix also showed significant weakening of the rheological properties of the nanocomposites [19]. Therefore, a larger polymer concentration in the matrix is desirable for successful templating and to maintain the mechanical properties of the matrix material. Silica particles that are larger than the interstitial cavity were found to have little effect on the rheology of the nanocomposites. It is also apparent in Fig. 7 that the relative location of these particles in space is not affected by the formation of the crystal structure around them. The scattering of the large particles in the fluid sample and the crystal is identical.

The effectiveness of the templating of the silica nanoparticles is also influenced by the absolute temperature of the samples. The temperature dependence of $S(Q)$ for the templated particles is shown in Fig. 7. It is found that temperature has a large effect for samples containing low polymer concentrations in the

matrix. As the temperature is raised from 35 °C to 65 °C the structure factor of the sample containing 20 wt.% F127 becomes flat for most of the Q range with the exception of a small valley around $Q = 0.034$ Å^{-1}. The existence of this valley is attributed to the presence of the micelles that affect the average separation distance between the nanoparticles. The sample that contains 25 wt.% in the matrix also shows a decrease in templating, as judged by the correlation of the $S(Q)$ peak with the peak of the polymer matrix. When the temperature of this sample is raised from 25 °C to 65 °C the peak shifts significantly to lower Q values and deviates from the peak of the polymer crystal (arrow). The stiffness of the cubic crystals is non-monotonic at temperatures above the order–disorder transition [19]. The modulus increases up to its maximum value at ∼45 °C and then begins to decrease. This temperature was found to be independent on polymer or silica concentration and we believe that it is related to the dehydration and collapse of the PEO corona. Although the template stiffness changes non-monotonically, the thermal motion of the nanoparticles increases steadily with temperature. Therefore, the temperature dependence is due to two competing effects, the increase in nanoparticle and micelle thermal motion and the dehydration of the PEO corona. From the data we conclude that the optimal temperature for nanoparticle templating is the lowest possible temperature above the gel transition.

Superlattices in binary hard sphere mixtures have been studied theoretically [21,22] and experimentally [23,24] with good agreement between models and observations. Although the particles (micelles and silica) in these nanocomposites are interacting, it is instructive to compare the observed phase behavior with that predicted for hard sphere mixtures. Deviations from hard-sphere interactions can shift the phase diagrams but the predictions should be roughly comparable to our system. This is because excluded volume interactions are the dominant factor in our system.

For the nanocomposites studied here, the hard sphere volume fraction of micelles lies between the freezing fraction and the close-packed fraction $0.54 < \phi_L < 0.74$ (FCC). Although determination of the exact hard-sphere fraction of micelles is not possible, we expect that this value is close to the upper limit ($\phi_L \sim 0.74$). This is suggested by the weak dependence of the lattice spacing of the neat micelle crystal (Fig. 2) with polymer concentrations above 20 w%. The range of studied volume fractions for the silica is known to be $0 < \phi_S < 0.05$. Comparison of our data to the phase diagram presented by Trizac et al. [22] for a hard sphere mixture with size ratio $\alpha = 0.414$ ($\alpha = 0.3$ in our system) shows that the expected stable phases in this concentration region are L + Fluid, LS + L, LS + L + Fluid, LS + Fluid, LS + S + Fluid and LS + S. Here, L is a pure FCC crystal of large particles, S is a pure crystal of small particles, LS is a NaCl-type crystal of large and small particles and Fluid is an amorphous fluid phase of large and small particles. For this size ratio or lower ($\alpha < 0.414$), no region of crystal phases with LS_2 lattice is predicted.

At low concentrations of small particles (silica) the stable phase in the phase diagram is LS + L. For the size ratio $\alpha = 0.414$, this phase persists up to $\phi_S \sim 0.05$ where the fluid phase begins to appear in coexistence with the others. However, lowering the size ratio to $\alpha = 0.3$ (that of our experiments) would change the transition boundary to lower concentrations of small particles [23]. Therefore, the predicted phase transition between the L + LS phase and a coexisting fluid phase would be in better quantitative agreement with the transition observed in our system ($\phi_S \sim 0.03$) [18]. Although the systems cannot be compared exactly, the observed behavior is qualitatively consistent with that predicted by theory. It is interesting to point out that phase coexistence occurs at all concentrations in this region. Experiments carried out in a larger colloidal system over a wide composition space showed that amorphous fluids dominated the phase space ($\alpha \sim 0.4$) with the exception of the limits of many large or many small particles [23]. Phase separation in binary crystals can occur spontaneously to minimize the interfacial area when the crystal lattices are very different and interfacial tension is high. In fact, pure LS phase (purely NaCl crystal) does not occur as a region and is only present as a short line between the LS + L and the LS + S phases. This is a common property of nanocomposites made by mixing pre-made particles. In contrast, a purely LS phase could be created with relative ease by synthesizing the particles inside the ordered micelle crystal phase.

The work of Hunt et al. also highlights the importance of crystallization kinetics [23]. These authors point out that discrepancies between models and experiments are likely due to the exceedingly long equilibration times. For their relatively large particles (200–500 nm), crystallization and phase evolution was observed over several months. In contrast, the appearance and evolution of turbidity in our nanoscale system is observed in timescales of minutes to hours.

4.2. Influence of particles on cubic matrix

The effect that nanoparticle additives have on micelle cubic crystals is of equal importance to potential applications as is the templating. Although for most samples the cubic structure of the micelle crystal is maintained, it was found that this structure was significantly altered by key experimental parameters. The relative number of particles to template sites was found to directly affect the relative intensities of the first and second diffraction peaks (see Figs. 10 and 11). The nonlinear change in the peak ratio (I_2/I_1) with particle concentration is a sign of alterations in the long range order of the micelle cubic crystal. At lower silica concentrations (<4 wt.%), the second peak intensity increases relative to the first while the position of the peak moves slightly toward lower Q. We interpret this as a sign of increased order and swelling of the micelle crystal due to the intercalated nanoparticles. When the concentration is increased further, we observe a discontinuous decrease of the peak ratio (I_2/I_1). At 10 wt.% silica (Fig. 10) the second "peak" becomes much softer and less well defined. This is a clear indication of the loss of long range structure as fewer areas of the sample satisfy Bragg's diffraction law. At this point the scattering is more characteristic of a fluid state where micelles have little long range order but they are interacting strongly at small length-scales. Temperature also has a disordering effect on the micelle crystal as it had on the silica nanoparticles. This is shown in Fig. 11 as the decrease in the peak ratio (I_2/I_1) for all silica concentrations at 50 °C. The

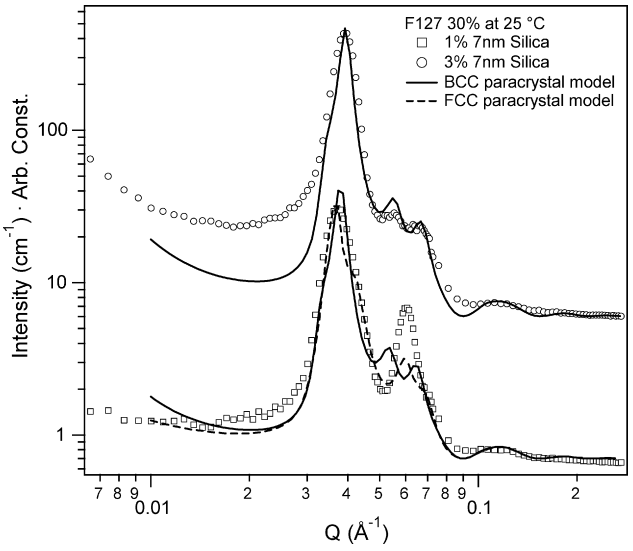

Fig. 12. Neutron scattering profiles for quiescent samples containing 30% F127 in the matrix with 1% (□) and 3% (◯) dispersed 7 nm silica particles. The solvent contains 58% D_2O so that the scattering from the cubic crystal matrix is measured. FCC (dashed line) and BCC (solid line) paracrystal models are also shown in the plots. The curve from the sample with 3% silica is shifted vertically for clarity.

fact that this ratio decreases more with the addition of silica suggests that the distortion is likely due to the thermal motion of the silica particles in the interstitial cavities.

An interesting observation was made when the silica concentration was increased from 1 wt.% to 3 wt.% in a sample containing 30 wt.% F127 in the matrix (Fig. 12). For all samples discussed up to this point the FCC lattice of the matrix was maintained. However, in this case we observe a transition from FCC to BCC with the addition of silica. This is observed as a change of the number of peaks and their relative position in the SANS profile. The peak positions in the BCC phase follow the expected $1{:}2^{1/2}{:}3^{1/2}$ while the FCC peaks are consistent with the $1{:}(4/3)^{1/2}{:}(8/3)^{1/2}{:}(11/3)^{1/2}$. However, the abundant imperfections in colloidal crystals and the instrumental resolution in SANS lead to a smearing effect that causes the combination of adjacent peaks into a single peak. This does not affect the BCC phase because the peaks are sufficiently far apart but it combines the first two (1 1 1) (2 0 0) and the last two peaks (2 2 0) (3 1 1) of the FCC crystal into two broad and asymmetric peaks. In the past, this effect has lead to a great deal of confusion in the determination of micelle crystal lattices. Therefore, to better show this transition we modeled the data using paracrystal structure factors with FCC and BCC periodicity and a sphere form factor [38]. The sample containing 3 wt.% silica was modeled with a BCC paracrystal using a micelle nearest neighbor distance (D_{HS}) of 19.5 nm, a micelle sphere radius of 5.0 nm (contrast of 2.1×10^{-6} Å^2) and a distortion factor of 0.095. The sample containing 1 wt.% silica was modeled with an FCC lattice using a micelle nearest neighbor distance (D_{HS}) of 21.0 nm, a micelle sphere radius of 5.0 nm (contrast of 2.1×10^{-6} Å^2) and a distortion factor of 0.12. Although the agreement in the absolute intensities is not perfect, the peak positions show that these are indeed FCC (1 wt.% silica) and BCC (3 wt.% silica) lattices. No combination of parameters was able to provide satisfactory fits for the 3 wt.% silica sample when either a FCC or simple cubic (SC) lattice was used. The same was true for the sample containing 1 wt.% silica when a BCC or SC lattice was used in the model. Even better model agreement with the data can be expected by using a micelle form factor that is more realistic (accounts for the scattering from the diffuse corona) and by accounting for other effects like finite crystal size and thermal distortions.

The cause for this transition remains unclear. BCC lattices have smaller interstitial cavities than FCC crystals and therefore this would seem to be unfavorable for the accommodation of intercalated particles. However, similar transitions from BCC to FCC and from FCC to BCC have been found to occur in polymer micelle cubic crystals as a function of temperature [39,40]. In these cases, the transitions were due to changes in the length-scale of the micelle interaction potential as the cores are swollen or the micelle corona contract. BCC crystals are more frequent in systems with short-range interaction potentials. Therefore, these crystal lattices are usually observed in more crowded environments. Unlike the previous observations of these transitions, the transition that we observe is due to the incorporation of nanoparticles. It is possible that the incorporation of particles into the lattice swells the particle-rich fraction of the cubic crystal sample. This in turn would cause the contraction of the particle-poor regions assuming that the number of micelles is conserved. This spatial contraction could trigger the transformation to BCC in the particle-poor region. Because the concentration of particles is still relatively low, the particle-poor region of the crystal is more abundant than the particle rich region and it dominates the scattering. Although this could be a plausible explanation for the transition, it puzzles us because the scattering from a sample containing 35 w% F127 is still consistent with an FCC periodicity.

5. Conclusions

We have reported on the influence of key design and experimental parameters on the templating of nanoparticles by polymeric micelle cubic crystals. The incorporation of significant quantities of nanoparticles into the interstitial cavities of these crystals is shown to be feasible. The long-range order of the cubic crystal is transferred indirectly to the nanoparticles by the excluded volume as the crystal is formed by raising the temperature. The thermo-reversible nature of the polymer allowed us to disperse pre-made charged particles without significant particle aggregation. We also show that shear can be used to orient the nanocomposites into a macro-crystal lattice. From these results we are able to formulate initial guidelines for the design of templated nanocomposites. It was found that the templating quality was better when the ratio of particles to interstitial sites is of order one or less. Above this number, the crystalline order of the matrix becomes distorted and there is less correlation between the structure of the particles and the template. It was also determined, as expected, that particles that are larger or comparable to the micelles will not be properly templated. Larger concentrations of polymer in the matrix resulted in stiffer crystals and increased nanoparticle organization. Increasing the temperature

far beyond the disorder–order transition was found to decrease order. The addition of particles also affected the structure of the micelle crystal. These initial observations will hopefully help guide the design of nanocomposite materials with controllable nanometer scale structure and macroscopic properties.

Acknowledgements

We wish to acknowledge the PPG foundation and National Science Foundation (CTS-9871110) for rheological equipment. DCP also acknowledges the PPG foundation for providing research funding. We are very grateful to Dr. Lionel Porcar (NIST) for his help during the SANS experiments and for his input in this work. This work utilized facilities supported in part by the National Science Foundation under Agreement No. DMR-9986442. We acknowledge the support of the National Institute of Standards and Technology, U.S. Department of Commerce, in providing the neutron research facilities used in this work.

References

[1] K. Mortensen, K. Almdal, D. Schwahn, F.S. Bates, Small-angle neutron scattering studies of the phase behavior and mesophases of homopolymers, block copolymers and complex mixtures, J. Appl. Crystallogr. 30 (1997) 702–707.
[2] P. Alexandridis, Poly(ethylene oxide) poly(propylene oxide) block copolymer surfactants, Curr. Opin. Coll. Interf. Sci. 2 (1997) 478–489.
[3] G. Wanka, H. Hoffmann, W. Ulbricht, Phase-diagrams and aggregation behavior of poly(oxyethylene)-poly(oxypropylene)-poly(oxyethylene) triblock copolymers in aqueous-solutions, Macromolecules 27 (1994) 4145–4159.
[4] L. Guo, R.H. Colby, M.Y. Lin, G.P. Dado, Micellar structure changes in aqueous mixtures of nonionic surfactants, J. Rheol. 45 (2001) 1223–1243.
[5] E. Eiser, F. Molino, G. Forte, X. Pithon, Flow in micellar cubic crystals, Rheol. Acta 39 (2000) 201–208.
[6] K. Mortensen, Structural studies of aqueous solutions of PEO–PPO–PEO triblock copolymers, their micellar aggregates and mesophases; a small-angle neutron scattering study, J. Phys.-Condens. Mater. 8 (1996) A103–A124.
[7] I.W. Hamley, Amphiphilic diblock copolymer gels: the relationship between structure and theology, Philos. T. Roy. Soc. A 359 (2001) 1017–1044.
[8] R.K. Prudhomme, G.W. Wu, D.K. Schneider, Structure and rheology studies of poly(oxyethylene-oxypropylene-oxyethylene) aqueous solution, Langmuir 12 (1996) 4651–4659.
[9] C.H. Wu, T.B. Liu, B.J. Chu, D.K. Schneider, V. Graziano, Characterization of the PEO–PPO–PEO triblock copolymer and its application as a separation medium in capillary electrophoresis, Macromolecules 30 (1997) 4574–4583.
[10] S. Forster, M. Antonietti, Amphiphilic block copolymers in structure-controlled nanomaterial hybrids, Adv. Mat. 10 (1998) 195.
[11] P.D. Yang, D.Y. Zhao, D.I. Margolese, B.F. Chmelka, G.D. Stucky, Generalized syntheses of large-pore mesoporous metal oxides with semicrystalline frameworks, Nature 396 (1998) 152–155.
[12] M.R. Bockstaller, E.L. Thomas, Proximity effects in self-organized binary particle-block copolymer blends, Phys. Rev. Lett. 93 (2004).
[13] K. Niesz, M.M. Koebel, G.A. Somorjai, Fabrication of two- and three-dimensional model catalyst systems with monodispersed platinum nanoparticles as active metal building blocks, Inorg. Chim. Acta 359 (2006) 2683–2689.
[14] R. Svingen, B. Akerman, Mechanism of electrophoretic migration of DNA in the cubic phase of pluronic F127 and water, J. Phys. Chem. B 108 (2004) 2735–2743.
[15] A. Katiyar, L. Ji, P. Smirniotis, N.G. Pinto, Protein adsorption on the mesoporous molecular sieve silicate SBA-15: effects of pH and pore size, J. Chromatogr. A 1069 (2005) 119–126.
[16] C.M. Coeshott, S.L. Smithson, E. Verderber, A. Samaniego, J.M. Blonder, G.J. Rosenthal, M.A.J. Westerink, Pluronic((R)) F127-based systemic vaccine delivery systems, Vaccine 22 (2004) 2396–2405.
[17] V.F. Puntes, P. Gorostiza, D.M. Aruguete, N.G. Bastus, A.P. Alivisatos, Collective behaviour in two-dimensional cobalt nanoparticle assemblies observed by magnetic force microscopy, Nat. Mater. 3 (2004) 263–268.
[18] D.C. Pozzo, L.M. Walker, Three-dimensional nanoparticle arrays templated by self-assembled block-copolymer gels, Macromol. Symp. 227 (2005) 203–210.
[19] D.C. Pozzo, K.R. Hollabaugh, L.M. Walker, Rheology and phase behavior of copolymer-templated nanocomposite materials, J. Rheol. 49 (2005) 759–782.
[20] P. Alexandridis, T.A. Hatton, Poly(ethylene oxide)-poly(propylene oxide)-poly(ethylene oxide) block-copolymer surfactants in aqueous-solutions and at interfaces—thermodynamics, structure, dynamics, and modeling, Coll. Surf. A—Physicochem. Eng. Aspects 96 (1995) 1–46.
[21] X. Cottin, P.A. Monson, Substitutionally ordered solid-solutions of hard-spheres, J. Chem. Phys. 102 (1995) 3354–3360.
[22] E. Trizac, M.D. Eldridge, P.A. Madden, Stability of the AB crystal for asymmetric binary hard sphere mixtures, Mol. Phys. 90 (1997) 675–678.
[23] N. Hunt, R. Jardine, P. Bartlett, Superlattice formation in mixtures of hard-sphere colloids, Phys. Rev. E 62 (2000) 900–913.
[24] A.E. Saunders, B.A. Korgel, Observation of an AB phase in bidisperse nanocrystal superlattices, Chemphyschem 6 (2005) 61–65.
[25] M. Malmsten, P. Linse, T. Cosgrove, Adsorption of Peo Ppo Peo block copolymers at silica, Macromolecules 25 (1992) 2474–2481.
[26] J.A. Shar, T.M. Obey, T. Cosgrove, Adsorption studies of polyethers—Part II: adsorption onto hydrophilic surfaces, Coll. Surf. A 150 (1999) 15–23.
[27] L.P. Stratton, A.C. Dong, M.C. Manning, J.F. Carpenter, Drug delivery matrix containing native protein precipitates suspended in a poloxamer gel, J. Pharmaceut. Sci. 86 (1997) 1006–1010.
[28] J. Laven, H.N. Stein, The electroviscous behavior of aqueous dispersions of amorphous silica (Ludox), J. Coll. Interf. Sci. 238 (2001) 8–15.
[29] G.C. Straty, H.J.M. Hanley, C.J. Glinka, Shearing apparatus for neutron-scattering studies on fluids—preliminary-results for colloidal suspensions, J. Stat. Phys. 62 (1991) 1015–1023.
[30] W.L. Griffith, R. Triolo, A.L. Compere, Analytical scattering function of a polydisperse Percus-Yevick fluid with Schulz-(gamma-) distributed diameters, Phys. Rev. A 35 (1987) 2200–2206.
[31] A. Guinier, X-Ray Diffraction, Freeman, London, 1963.
[32] V.F. Sears, Neutron scattering lengths and cross sections, Neutron News 3 (1992) 26–37.
[33] W. Loose, B.J. Ackerson, Model-calculations for the analysis of scattering data from layered structures, J. Chem. Phys. 101 (1994) 7211–7220.
[34] J.P. Habas, E. Pavie, A. Lapp, J. Peyrelasse, Understanding the complex rheological behavior of PEO–PPO–PEO copolymers in aqueous solution, J. Rheol. 48 (2004) 1–21.
[35] H. Matsuoka, H. Tanaka, T. Hashimoto, N. Ise, Elastic-scattering from cubic lattice systems with paracrystalline distortion, Phys. Rev. B 36 (1987) 1754–1765.
[36] H. Matsuoka, H. Tanaka, N. Iizuka, T. Hashimoto, N. Ise, Elastic-scattering from cubic lattice systems with paracrystalline distortion. 2, Phys. Rev. B 41 (1990) 3854–3856.
[37] J.K. Percus, G.J. Yevick, Analysis of classical statistical mechanics by means of collective coordinates, Phys. Rev. 110 (1958) 1–13.
[38] A. Guinier, G. Fournet, Small-Angle Scattering from X-rays, John Wiley and Sons, New York, 1955.
[39] J. Bang, T.P. Lodge, X.H. Wang, K.L. Brinker, W.R. Burghardt, Thermoreversible, epitaxial fcc ⟨−⟩ bcc transitions in block copolymer solutions, Phys. Rev. Lett. 89 (2002).
[40] I.W. Hamley, J.A. Pople, O. Diat, A thermally induced transition from a body-centred to a face-centred cubic lattice in a diblock copolymer gel, Coll. Polym. Sci. 276 (1998) 446–450.